Available online at www.sciencedirect.com

SCIENCE DIRECT

Experimental and Molecular Pathology 79 (2005) 14 – 22

Experimental and Molecular Pathology

www.elsevier.com/locate/yexmp

Quantitative multi-gene transcriptional profiling using real-time PCR with a master template☆

Shu-Ching Shih[a,*], Lois E.H. Smith[b]

[a]Pathology Department, Beth Israel Deaconess Medical Center, Harvard Medical School, 99 Brookline Avenue, Boston, MA 02215, USA
[b]Ophthalmology Department, Children's Hospital, Harvard Medical School, 300 Longwood Avenue, Boston, MA 02115, USA

Received 3 March 2005
Available online 13 May 2005

Abstract

We previously reported a method for quantitative multi-gene transcriptional profiling with gene-specific standard curves using real-time PCR. Here, we report an approach that increases experimental throughput by using a master template to generate a single standard curve for the estimation of mRNA copy numbers from all genes. We prepared fifty-nine different templates and measured eNOS mRNA copy numbers in Matrigel VEGF-transfectant samples. The copy numbers obtained using each of the fifty-nine templates were within 50% of the copy number obtained using the previously reported method. Analysis of primer design parameters, and subsequent tests, showed that eliminating complementarities between the first nucleotides at the 5′-ends of the forward and reverse primers reduces the influence of saturation effects and produces copy numbers similar to those generated with gene-specific templates—generally, within 20%. Measurements on a panel consisting of eNOS, iNOS, and nNOS further validated the master-template approach. The master-template approach enables rapid quantification of mRNA abundances from panels of hundreds of genes, and will be a valuable tool for screening large numbers of genes as part of a search for biomarkers, the validation of DNA-microarray data, or research into the dynamics of the gene–protein network.
© 2005 Elsevier Inc. All rights reserved.

Keywords: Real-time PCR; Transcriptional profiling; mRNA copy number; Tissue fingerprinting; Gene expression

Introduction

Multi-gene transcriptional profiles provide a quantitative view of the expression of many genes (Shih et al., 2002); they thus provide a window into the overall state of the gene network, and are valuable for fingerprinting biological processes (Shih et al., 2003a,b). A significant fraction of the genome is differentially expressed in pathological tissue versus normal tissue (Alizadeh et al., 2000; Rickman et al., 2001; Simkhovich et al., 2003), suggesting that hundreds or thousands of genes will ultimately be found to "mark" any particular disease.

Functional genomics studies have demonstrated a tight correlation between the functioning of a protein and the expression of its gene (Brown and Botstein, 1999). Thus, techniques like DNA-microarrays, which screen the entire genome, have been widely used to find genes critically involved in disease processes (Clarke et al., 2001). Unfortunately, DNA-microarrays are limited in their accuracy, making them potentially unreliable in measuring differential gene expression (Bassett et al., 1999; Ding and Cantor, 2004). Reproducibility is also a question, as arrays from different companies have been shown to produce different results (Mah et al., 2004; Yauk et al., 2004). Thus, it is important to use techniques like real-time PCR, a method widely regarded as the gold standard for nucleic acid quantification (Heid et al., 1996; Jung et al., 2000; Klein, 2002), to validate DNA-microarray data (Crnogorac-Jurcevic et al., 2002; Rickman et al., 2001; Miyazato et al., 2001). However, conventional real-time PCR analysis, which mainly focuses on measuring the fold differences of expression of each gene, does not address inter-gene relationships. Precisely quantifying mRNA copy

☆ Grants: EY08670, EY14811 and the V Kann Rasmussen Foundation.
* Corresponding author. Fax: +1 617 667 3591.
E-mail address: sshih2@bidmc.harvard.edu (S.-C. Shih).

0014-4800/$ - see front matter © 2005 Elsevier Inc. All rights reserved.
doi:10.1016/j.yexmp.2005.03.004

numbers from multi-gene panels using real-time PCR, so that abundances can be reliably compared across genes (Shih et al., 2002), enables exploration of these inter-gene relationships and furthers our understanding of the systems biology underlying disease development.

A significant limitation of our previously reported technique (Shih et al., 2002), however, arose from the need to clone a specific cDNA template for every gene and to generate a standard curve for each gene to be measured in every PCR run. This diminishes experimental throughput and also risks introducing new sources of cross-gene and cross-run data variability. We therefore investigated whether a single template for many genes – a master template – can reliably be used to measure copy numbers for all genes in a panel. Because standard curve parameters vary with PCR amplification efficiencies and saturation effects (Jung et al., 2000; Liu and Saint, 2002; Wilhelm and Pingoud, 2003), a master template will function within experimental margins of error if primers for different genes can be made sufficiently uniform in their amplification efficiencies and saturation effects.

To evaluate the master-template approach, we prepared fifty-nine different cDNA templates and their specific primers, and measured endothelial nitric oxide synthases (eNOS) mRNA copy numbers from Matrigel VEGF-transfectants. Our study supports the notion that the master-template approach is reliable for mRNA copy number measurement for all genes if primers are properly designed, and offers a fast and high-throughput alternative to gene-specific standard-curve quantification in multi-gene transcriptional profiling.

Materials and methods

Skin angiogenesis model

Human SK-MEL melanoma cells were transfected with human $VEGF_{165}$ under the direction of a CMV promoter and clones of VEGF-Low and VEGF-High transfectants were isolated (Shih et al., 2002). Athymic NCr nude mice (7–8 weeks old, females) were injected subdermally midway on the right and left back sides with 0.25 ml Matrigel (BD Biosciences, San Jose, CA) at a final concentration of 10 mg/ml protein either alone to produce a control, or with 1.5×10^6 SK-MEL-VEGF-High or -VEGF-Low transfectants. Soon after injection, the Matrigel implant solidified, and persisted without apparent deterioration throughout the 6-day assay interval. After 6 days, the animals were euthanized, and skin specimens were harvested after removal of Matrigel.

RNA isolation and cDNA preparation

Upon dissection, the implanted Matrigel specimens were removed and total RNA was prepared from the skin that was beneath the Matrigel using the RNeasy RNA extraction kit (Qiagen, Chatsworth, CA). Briefly, tissues were lysed in guanadinium isothiocyanate buffer and RNA was purified following manufacturer's instruction. The purified RNA was suspended in RNase free H_2O. Before cDNA was generated, total RNA (1 μg) was treated with DNase I (Ambion, Austin, Tex.) to remove contaminating genomic DNA. The DNase-treated RNA (100 ng) was then converted into cDNA by using random primers and SuperScript III (Invitrogen, Bethesda, MD). All cDNA samples were diluted to 100 μl with H_2O, aliquoted, and stored at −80°C.

cDNA template construction and preparation

For each of fifty-nine different human and mouse genes, we cloned a 350- to 550-bp-long cDNA fragment that bracketed both real-time PCR primers. The fragments were cloned from either a mouse embryo or a human liver cDNA library (BD Biosciences) and inserted into PCRScript vectors (Strategene, La Jolla, CA). Each cDNA template was purified using Strategene's Plasmid Extraction Kit and phenol/chloroform extraction to remove protein contaminants, precisely quantified, and tenfold serially diluted to produce a series in which the lowest-concentration dilution has a single copy per microliter. Real-time PCR with SYBR Green I (Qiagen) was used to produce a standard curve for each of the fifty-nine serially diluted cDNA template series. SYBR Green I, which binds sequence-independently to the minor groove of dsDNA and generates 1000-fold higher fluorescence than in its free state, has a wide dynamic range that in PCR reactions extends from less than 10 copies per well to more than 10^7 copies per well (Morrison et al., 1998; Wittwer et al., 1997). To produce a standard curve, the threshold cycle (Ct) values for each dilution in the template series are plotted as a function of the logarithm of the known input template numbers and a linear trendline is fitted to the data (Table 1).

Real-time PCR primer design and validation

We followed the guidelines of the Primer Express oligo design software (Applied BioSystems, Foster City, CA). Specific areas of the gene sequence were selected for primer design based on successive NCBI Blast searches to eliminate regions with significant homologies to other genes. Primers are designed to meet standard primer design parameters, including the lowest possible melting temperature difference, with melting temperatures in the range 58–60°C. Where feasible, the 3′-end of the primers finishes in a pyrimidine nucleotide (G or C), but 3 out of 5 of the 3′-end nucleotides are A or T. Primers are 19–25 bp in length and amplicons are typically 60–110 bp long. All primer sets are then re-checked via NCBI short oligonucleotide blast database searches to identify potential conflicting transcript matches. Primers were synthesized by Genemed Synthesis (South San Francisco, CA). The sequences of all

Table 1
Real-time PCR template, primer, amplicon, and standard curve parameters

Gene symbol	cDNA (bp)	Real-time PCR primer: forward				Real-time PCR primer: reverse				Amplicon (bp)	Trendline	R^2	E (%)
		Sequence	Length	% GC	Tm	Sequence	Length	% GC	Tm				
0–20% Difference													
Mm Cdh5	505	**T**CCTCTGCATCCTCACTATCACA	23	47.8	58	**G**TAAGTGACCAACTGCTCGTGAAT	24	45.8	58	122	$y = -3.4918x + 35.494$	0.9968	93.4
Mm Gfap	514	**G**CTGGAGGGCGAAGAAAAC	19	57.9	58	**T**GGCCTTCTGACACGGATTT	19	52.6	59	102	$y = -3.5040x + 35.815$	0.9956	92.9
Mm Igfbp2	510	**G**CCCCCTGGAACATCTCTACT	21	57.1	58	**T**CCGTTCAGAGACATCTTGCA	21	47.6	58	92	$y = -3.5718x + 36.31$	0.9997	90.5
Mm Pecam1	501	**G**AGCCCAATCACGTTTCAGTTT	22	45.5	59	**T**CCTTCCTGCTTCTTGCTAGCT	22	50.0	59	118	$y = -3.4409x + 35.416$	0.9991	95.3
Mm Sele	501	**T**TGAGTGCACATCTCAGGGAAA	22	45.5	59	**G**ACGTCAAGGCTTGGACATTG	21	52.4	59	77	$y = -3.4204x + 35.735$	0.9996	96.0
Mm Plau	501	**G**AAGTCCTCCCTCCTTTAAATGTG	24	45.8	58	**T**GGGAGTTGAATGAAGCAGTGT	22	45.5	58	86	$y = -3.4345x + 36.426$	0.9993	95.5
Hs PTGS2	510	**G**GTCTGGTGCCTGGTCTGAT	20	60.0	59	**T**GTTTAAGCACATCGCATACTCTGT	25	40.0	59	77	$y = -3.4813x + 35.665$	0.9988	93.8
Hs FGF2	600	**T**TCGGCATGTAGCTCATGATCTAT	24	41.7	59	**G**CAGGGCAGATTTGCTCACTA	21	52.4	59	79	$y = -3.5039x + 36.099$	0.9995	92.9
Mm Ptgs2	503	**G**GGTGTCCCTTCACTTCTTTCA	22	50.0	59	**G**GCGCTTGCATTGATGGT	18	55.6	59	71	$y = -3.5252x + 35.826$	0.9982	92.2
Mm Nos2	504	**G**GTGTTCTTTGCTTCCATGCTAAT	24	41.7	60	**G**TCCCTGGCTAGTGCTTCAGA	21	57.1	58	106	$y = -3.4732x + 36.169$	0.9961	94.1
Mm Nos1	506	**G**GACTGATGGCAAGCATGACT	21	52.4	60	**G**CCCAAGGTAGAGCCATCTG	21	61.9	58	89	$y = -3.4366x + 35.543$	0.9985	95.4
Mm Vegfa	502	**G**GAGACTCTTCGAGGAGCACTT	22	54.5	60	**G**GCGATTTAGCAGCAGATATAAGAA	25	40.0	59	80	$y = -3.4882x + 36.019$	0.9986	93.5
Mm Flt1	508	**G**TCACAGAGGAGGATGAGGGTG	22	59.1	59	**G**TGAGGTAGGCTGCGCTTTC	20	60.0	58	116	$y = -3.4903x + 36.603$	0.9980	93.4
Hs SERPINE1	511	**G**GCTGACTTCACGAGTCTTTCAG	23	56.5	59	**G**TTCACCTCGATCTTCACTTTCTG	24	45.8	58	79	$y = -3.4418x + 35.308$	0.9922	95.2
Hs TIE1	504	**G**CCTGGGCCAATATCCAAGT	20	55.0	60	**G**CCTGTCCACGTCTATCCACA	21	57.1	60	83	$y = -3.4938x + 35.549$	0.9985	93.3
Mm Plat	502	**C**GACACAATTATTGTCGGAATCC	23	43.5	59	**C**ACGTCAGCTTTCGGTCCTT	20	55.0	59	77	$y = -3.5703x + 36.638$	0.9972	90.6
Hs PPIA	510	**C**TGGACCCAACACAAATGGTT	21	47.6	59	**C**CACAATATTCATGCCTTCTTTCA	24	37.5	59	111	$y = -3.4629x + 35.028$	0.9974	94.4
Hs IGF1	507	**C**TTCCGGAGCTGTGATCTAAGG	22	54.6	59	**C**GGACAGAGCGAGCTGACTT	20	60.0	59	78	$y = -3.5468x + 36.229$	0.9967	91.4
Hs ANGPT1	407	**C**GCTGCCATTCTGACTCACATA	22	50.0	60	**C**CGGTTATATCTTCTCCCACTGTTT	25	44.0	60	76	$y = -3.6200x + 37.178$	0.9992	90.0
Hs FGFR1	522	**C**GTGGAGTTCATGTGTAAGGTGTAC	25	48.0	58	**C**CATTCACCTCGATGTGCTTT	21	47.6	58	75	$y = -3.5745x + 36.267$	0.9953	90.4
Mm Ppia	402	**C**AGACGCCACTGTCGCTTT	19	57.9	59	**T**GTCTTTGGAACTTTGTCTGCAA	23	39.1	59	133	$y = -3.4220x + 35.483$	0.9972	96.0
Mm Igf1	501	**T**CATGTCGTCTTCACACCTCTTCT	24	45.8	59	**C**CACACACGAACTGAAGAGCAT	22	50.0	59	124	$y = -3.5505x + 36.463$	0.9994	91.3
Mm Igfbp3	439	**C**CGAGTCTAAGCGGGAGACA	20	60.0	59	**T**CAGCACATTGAGGAACTTCAGA	23	43.5	59	87	$y = -3.4370x + 36.097$	0.9995	95.4
Hs SELE	545	**T**TCCGGGAAAGATCAACATGA	21	42.9	59	**C**ATTGAGCGTCCATCCTTCA	20	50.0	58	90	$y = -3.5350x + 36.538$	0.9921	91.8
Hs FLT1	505	**C**CCTCGCCGGAAGTTGTAT	19	42.1	59	**T**TAACGAGTAGCCACGAGTCAAAT	24	41.7	58	85	$y = -3.4230x + 35.065$	0.9995	95.9
Mm Epnb2	503	**A**TGCATCATCTTCATCGTCATCA	23	39.1	59	**T**GGAGAGTGTTTGCGGTGTCT	21	52.4	59	82	$y = -3.4823x + 36.02$	0.9988	93.7
Mm Nos3	576	**T**GAAGATCTCTGCCTCACTCATG	23	47.8	58	**A**GTCTCAGAGCCATACAGAATGGTT	25	44.0	58	77	$y = -3.5489x + 35.990$	0.9981	91.3
Hs TGFB2	503	**T**GCTAATGTTATTGCCCTCCTACA	24	41.7	59	**A**ATAGGCCGCATCCAAAGC	19	52.6	59	81	$y = -3.5430x + 36.337$	0.9983	91.5
Hs TIE2	386	**A**AGCGGCCTAGGACAGAACAT	21	52.4	59	**T**TCTCAGCAGTTGTCAAGGGTCT	23	47.8	59	79	$y = -3.5566x + 37.389$	0.9992	91.1

Mm Angpt2	504	**T**TAGCACAAAGGATTCGGACAAT	23	39.1	59	**T**TTTGTGGGTAGTACTGTCCATTCA	25	40.0	59	121	$y = -3.5075x + 35.692$	0.9979	92.8
Hs NPR1	501	**T**GAAAAATGCGAATGGCTGAT	21	38.1	59	**T**CGAAGTGAGGGTTGAAGTTGA	22	45.5	58	74	$y = -3.4714x + 35.946$	0.9967	94.1
Hs IGFBP1	521	**T**GGATTTTATCACAGCAGACAGTGT	25	40.0	59	**T**GGAGACCCAGGGATCCTCT	20	60.0	59	103	$y = -3.5566x + 36.491$	0.9999	91.1
Mm Tie1	533	**C**AAGGTCACACACACGGTGAA	21	52.4	59	**G**CCAGTCTAGGGTATTGAAGTAGGA	25	48.0	58	122	$y = -3.5789x + 36.262$	0.9990	90.3
Hs VEGF	568	**G**CGGAGAAAGCATTTGTTTGT	21	42.9	58	**C**GGCTTGTCACATCTGCAA	19	52.6	58	124	$y = -3.5379x + 36.669$	0.9990	91.7
Hs KDR	543	**C**GGCAAATGTGTCAGCTTTG	20	50.0	59	**G**GTCACGTGGAAGGAGATCAC	22	54.6	59	83	$y = -3.4714x + 35.946$	0.9967	100.1
Ms Tie2	502	**A**CTCTTCATGTACAACGGCCATT	23	43.5	59	**A**GTGGGTGGCTTGCTTGGTA	20	55.0	59	76	$y = -3.5654x + 36.479$	0.9992	90.8
Hs MCAM	561	**A**GGAACACAGTGGGCGCTAT	20	55.0	58	**C**TCACTCGGACGTCAGACACA	21	57.1	58	112	$y = -3.5593x + 36.016$	0.9976	91.0
20–50% Difference													
Mm Rplp1	376	**C**AGTCTACAGCATGGCTTCCG	21	57.1	59	**G**TGACCGTCACCTCGTCGT	19	63.2	58	82	$y = -3.2780x + 34.924$	0.9983	101.9
Mm Angpt1	502	**C**ATTCTTCGCTGCCATTCTG	20	50.0	58	**G**CACATTGCCCATGTTGAATC	21	47.6	60	103	$y = -3.1985x + 34.42$	0.9963	105.4
Mm Fn1	290	**G**CTCACTGACCTAAGCTTTGTTGA	24	45.8	59	**C**CGATAATGGTGGAAGAGTTTAGC	24	45.8	59	84	$y = -3.3991x + 35.964$	0.9984	96.9
Mm Xlkd1	451	**C**TGTCATCCCTCGGATTTTCTC	22	50.0	59	**G**GAGGGAGCATTCCAAATCAG	21	52.4	59	77	$y = -3.3853x + 35.935$	0.9994	97.4
Mm Timp1	455	**C**AAACTGGAGAGTGACACTCACTGT	25	48.0	59	**G**CAAAGTGACGGCTCTGGTAGT	22	54.6	59	81	$y = -3.3412x + 35.381$	0.9977	99.2
Hs IGF1R	456	**G**GCAGCCAGAGCATGTACTG	20	60.0	58	**C**CCTTGAAGATGGTGCATCCT	21	52.4	60	121	$y = -3.3995x + 35.898$	0.9989	96.9
Mm Kdr	519	**G**CCCTGCTGTGGTCTCACTAC	21	61.9	58	**C**AAAGCATTGCCCATTCGAT	20	45.0	59	116	$y = -3.3186x + 34.944$	0.9962	100.1
Hs PLAU	507	**G**GAAAACCTCATCCTACACAAGGA	24	45.8	59	**C**GGATCTTCAGCAAGGCAAT	20	50.0	59	77	$y = -3.4066x + 35.248$	0.9989	96.6
Mm Igfbp4	518	**T**TCATCATCCCCATTCCAAAC	21	42.9	58	**A**CCCCTGTCTTCCGATCCA	19	57.9	59	116	$y = -3.3336x + 34.728$	0.9988	95.5
Mm Nrp1	502	**T**GAGGAAGTTCAAGATCGCCTATA	24	41.7	58	**A**AGCTCAGGTGTGTCATAGTTGTTG	25	44.0	58	119	$y = -3.3834x + 34.904$	0.9959	97.5
Hs ANGPT2	508	**A**GCATGGGTCCTGCAGCTA	19	57.9	58	**T**GCACAGCATTGGACACGTA	20	50.0	58	88	$y = -3.3389x + 34.962$	0.9996	99.3
Mm Igf1r	513	**G**AAAACTGCACGGTGATCGA	20	50.0	58	**A**GCAGCAAGTACTCGGTGATGA	22	50.0	59	113	$y = -3.2518x + 34.097$	0.9939	103.0
Mm Igfbp1	501	**G**CGATGCCCGAGTTCCTAA	19	57.9	60	**A**GCAGTGCAGGGAGCACAGT	20	60.0	60	114	$y = -3.3111x + 34.924$	0.9984	100.5
Mm Flt3l	401	**C**AGGACGAGAAGCACTGCAA	20	55.0	59	**C**CCTGCCACAGTCTTCAGTTG	21	57.1	59	81	$y = -3.3455x + 35.362$	0.9961	99.0
Hs FN1	501	**C**AACTCACTGACCTAAGCTTTGTTG	25	44.0	59	**C**GGTACCCAATAATGGTGGAA	21	47.6	58	92	$y = -3.3186x + 35.078$	0.9981	100.1
Mm Ephb4	503	**G**CAATGGGAGGGAAGTTGAGTAC	23	52.2	60	**T**GCCTCATTAGGGTCTTCGTAAG	23	52.2	58	107	$y = -3.3879x + 35.703$	0.9996	97.3
Mm Mcam	405	**G**TCAGATAAGCTCCCAGAAGAGATG	25	48.0	59	**T**GTATTTCTCTCCCTGGTCTCCTG	24	50.0	60	86	$y = -3.2609x + 34.670$	0.9948	102.6
Hs CDH5	512	**G**AACCCAAGATGTGGCCTTTAG	22	50.0	59	**G**ATGTGACAACAGCGAGGTGTAA	24	45.8	59	103	$y = -3.3605x + 34.852$	0.9991	98.4
Mm Mmp9	504	**A**CTGCGGGCTCTTCTGAGG	19	63.2	59	**C**CCTGGATCTCAGCAATAGCA	21	52.4	59	96	$y = -3.3973x + 35.824$	0.9991	96.9
Mm Igfbp5	504	**G**ATGAGACAGGAATCCGAACAAG	23	47.8	59	**A**ATCCTTTGCGGTCACAGTTG	21	47.6	59	125	$y = -3.5759x + 36.099$	0.9997	90.4
Mm B2m	341	**G**ATACATACGCCTGCAGAGTTAAGC	25	48.0	59	**A**TCACATGTCTCGATCCCAGTAGA	24	45.8	59	76	$y = -3.4721x + 34.633$	0.9943	94.1
Mm Acta2	519	**A**CCGCTGCCTCTTCCTCCT	19	63.2	60	**G**GCAACGGAAACGCTCATT	19	52.6	60	88	$y = -3.4798x + 36.486$	0.9978	93.8

Mm, *Mus musculus*; Hs, *Homo sapiens*; cDNA (bp), the size of cDNA insert in each clone plasmid; primer information: forward and reverse primer sequences, length of each primer, % GC content in each primer (% GC), primer melting temperature (Tm), and the size of PCR product in real-time PCR (amplicon); standard curve information: trendline of each standard curve, R^2 value, and PCR efficiency (E). The genes are listed in two categories depending on whether the discrepancy in eNOS copy number obtained using the template varied by more or less than 20% from that obtained with the eNOS-specific template.

real-time PCR primers used in this paper are listed in Table 1 (5′ to 3′). To assure the specificity of each primer set, amplicons generated from PCR reaction were analyzed for specific melting point temperatures by using the first derivative primer melting curve software supplied by Applied BioSystems.

TaqMan quantitative real-time PCR

The SYBR Green I assay and the ABI Prism 7700 Sequence Detection System were used for detecting real-time PCR products from reverse transcribed Matrigel cDNA samples and performed as described previously (Shih et al., 2002). Although 18S rRNA is a desirable endogeneous control (Thellin et al., 1999), the 18S rRNA transcript is almost 2^{12} to 2^{30} times more abundant than most other mRNAs and is therefore inappropriate to use as a housekeeping gene. We used cyclophilin-A, which exhibits a constant level in the Matrigel samples in comparison with 18S rRNA, as the normalizer. PCR reactions for each Matrigel cDNA sample (6 μl) were performed in duplicate for both eNOS and cyclophilin-A, and copy numbers were calculated using standard curves generated from each of the fifty-nine cDNA templates. The level of target gene expression was normalized against the cyclophilin-A expression in each sample and the data presented as mRNA copies/10^6 cyclophilin-A copies.

Data analysis—standard method and master-template method

In the standard method, standard curves are created using a gene-specific cDNA template and gene-specific primers for every gene including the housekeeping gene (Shih et al., 2002). The mRNA copy numbers for each gene in each sample are then calculated through their respective standard curve. To obtain a normalized abundance, mRNA copy numbers of each gene are divided by the mRNA copy number of the housekeeping gene measured in an equal quantity of the same sample. As real-time PCR is sensitive to various experimental parameters such as pipetting errors and the choice of fluorescence threshold used to determine the threshold cycles, Ct, it is not unusual to obtain a 20% variation in copy number from different runs observing a particular gene and sample.

In the master-template approach, a single standard curve is created using one selected reference cDNA template and its specific primers known to produce good standard curves. Good standard curves have a close linear fit across multiple orders of dilution, with little change in calculated slope and intercept if a different dilution range is selected; are consistent across PCR runs; have a slope between 3.35 and 3.55; and are derived from fluorescence curves which show few signs of significant saturation at Ct for any dilution. The reference template need not be the same as the housekeeping gene or the genes under study. The number of mRNA copies for each gene-sample combination is calculated using this one standard curve. To obtain a normalized abundance, copy numbers of the gene of interest (obtained using the reference-gene standard curve) are divided by copy numbers of the housekeeping gene (also obtained using the reference-gene standard curve).

Results

Measurement of eNOS mRNA copy numbers in SK-MEL human melanoma VEGF-transfectants induced neovascularization

Angiogenesis requires the elaboration of endothelium-derived nitric oxide (NO) and angiogenic factors like VEGF induce the release of NO from endothelial cells (Hood et al., 1998; van der Zee et al., 1997). Using a Matrigel VEGF-transfectant model that serves as a well-controlled source of neovascularization for identification of mRNAs that correlate with VEGF expression and angiogenesis (Shih et al., 2002), we measured the expression level of eNOS. Cyclophilin-A, a primary cytosolic receptor for cyclosporine A (Trandinh et al., 1992) that showed uniform expression in the Matrigel samples (data not shown), was used as a normalizer. Both eNOS and cyclophilin-A standard curves were generated from their respective templates and primers (*Mm Nos3* and *Mm Ppia* in Table 1) and measured mRNA copy numbers of the respective target gene in Matrigel samples. VEGF-High transfectants, which produce a VEGF level 5 times higher than that produced by VEGF-Low transfectants (Shih et al., 2002), induced a significantly greater degree of skin angiogenesis than the VEGF-Low transfectants and the Matrigel alone (Fig. 1a). The skin specimens with VEGF-High transfectants also demonstrated higher copy numbers of eNOS than skin specimens with the VEGF-Low transfectants or the Matrigel alone; eNOS mRNA copies per 10^6 cyclophilin copies for the VEGF-High, VEGF-Low, and control Matrigels were 28,230 ± 1424, 7020 ± 868, and 4544 ± 250, respectively (Fig. 1b). Thus, relative to the control Matrigel, the VEGF-High Matrigel had a 6.2-fold induction of eNOS mRNA level, whereas the VEGF-Low Matrigel had a 1.6-fold induction.

Measurement of eNOS mRNA copy numbers through standard curves generated from fifty-nine cDNA templates in real-time PCR

To explore the possibility of using a master template to generate standard curves in real-time PCR and measure all other target gene copy numbers, fifty-nine different cDNA templates were prepared (Table 1). These templates, which have 350–550 bp cDNA inserts of either mouse or human genes, were precisely quantified and 10-fold serially diluted. Specific real-time PCR primers were designed for each of the fifty-nine cDNA templates (Table 1), and used to

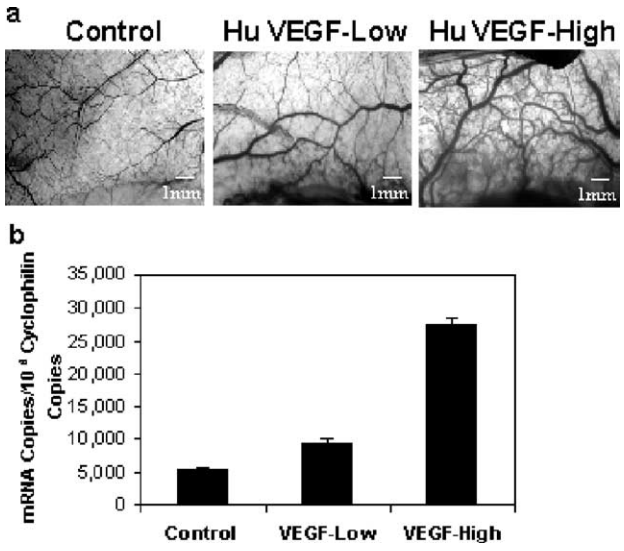

Fig. 1. Real-time quantitative RT-PCR measurement of eNOS expression using standard curves derived from eNOS-specific cDNA templates. (a) Angiogenesis in nude mouse skin was induced by subdermal injection of Matrigel itself (Control) or Matrigel containing 1.5×10^6 cells of VEGF-Low or VEGF-High transfectants. Tissues were harvested and photographed at day 6. (b) Quantitative real-time PCR measurement of eNOS copy numbers using precisely measured and 10-fold serially diluted eNOS and cyclophilin-A cDNA templates to generate standard curves. Control, VEGF-Low, and VEGF-High, respectively, showed 4544 ± 250, 7020 ± 868, and 28,230 ± 1424 eNOS mRNA copies/10^6 cyclophilin mRNA copies.

generate standard curves to measure both eNOS and cyclophilin-A mRNA. Linear regression analysis of all standard curves showed a high correlation (R^2 coefficient > 0.99), and measured PCR amplification efficiencies ranged between 90% and 103%. Since 20% variations in copy number for the same experiment are common using the standard method, in Table 1 the fifty-nine cDNA templates are grouped into two sets according to whether the difference in eNOS copy numbers between the standard and master-template approaches was less than 20% (i.e., insignificant) or greater than 20%. For example, eNOS mRNA copies per 10^6 cyclophilin copies for the VEGF-High, VEGF-Low, and control Matrigels were 26,045 ± 1336, 6377 ± 801, and 4088 ± 229 using the murine Cadherin-5 template (*Mm Cdh5*), a difference of less than 20% compared to the standard approach (Fig. 1), whereas the copy numbers were 20,528 ± 1121, 4587 ± 613, and 2856 ± 170 using the murine acidic ribosomal P1 template (*Mm Rplp*), a difference significantly larger than 20%. Within the two groups, templates were sorted by the 5′-end bases of their primers. Notably, no template gave a difference as large as 50%; forty templates yielded a difference of less than 20%.

Design of primer 5′-ends to eliminate complementarity improves consistency of non-specific standard curve quantification

We analyzed various primer characteristics in order to find characteristics that correlated with a low difference in estimated copy number between specific and master templates. Primarily because nearly all primers complied with known design rules, we found no correlation with such primer design parameters of ABI Primer Express as primer length, melting temperature, % GC content, 3′-end finish in a pyrimidine nucleotide, and 3 out of 5 of the 3′-end nucleotides A or T. We found that the first nucleotide combination at the 5′-ends of forward and reverse primers is strongly correlated with the difference in copy numbers. In Table 2, we show, for each combination of 5′-end bases of the forward and reverse primers, the number of primer sets with that combination giving less than 20% or greater than 20% differences in copy number. We found the following probabilities for a less than 20% difference: (1) **C**/**T**, all five cDNA templates, 100% probability; (2) **T**/**T**, all three cDNA templates, 100% probability; (3) **G**/**G**, seven out of eight cDNA templates, 87.5% probability; (4) **G**/**T**, eight out of ten cDNA templates, 80% probability; (5) **C**/**C**, five out of seven cDNA templates, 71.4% probability; (6) **G**/**A**, three out of five cDNA templates, 60% probability; (7) **A**/**T**, four out of seven cDNA templates, 57.1% probability; (8) **C**/**A** combination, one out of two cDNA templates, 50.0% probability; and (9) **C**/**G** combination, three out of eleven cDNA templates, 27.3% probability. Overall, primer sets whose first 5′-end nucleotides are complementary produce standard curves that give poor-quality quantification (only 7 of 18 templates with C/G or A/T combinations produced copy number differences less than 20%, a 38.9% probability). In contrast, non-complementary combinations appear to be less prone to quantification errors and to generate standard curves that more reliably estimate copy number (33 of 41 cases generated copy number differences less than 20%, an 80.5% probability). To verify that complementary at the 5′-ends increases quantification differences, we re-designed the primers for acidic ribosomal

Table 2
Probability of generating less than a 20% difference in copy number as a function of the 5′-end first base composition of real-time PCR primers

1st Base	Number of cDNA templates	Total number of cDNA templates	Probability
F/R	0–20% Difference	*n*	%
C/T	5	5	100.0
T/T	3	3	100.0
A/A	1	1	100.0
G/G	7	8	87.5
G/T	8	10	80.0
C/C	5	7	71.4
G/A	3	5	60.0
A/T	4	7	57.1
C/A	1	2	50.0
C/G	3	11	27.3

From Table 1, the number of cDNA templates which generated 0–20% difference in copy numbers was counted from each 5′-end first base primer composition. The probability was calculated by grouping genes in Table 1 according to 5′-end base pair combinations, and dividing the number of templates that gave less than a 20% difference in copy number with the total number of templates with that combination.

P1 (*Mm Rplp*) (Forward/Reverse: GAGCCACCAACCA-GAAGGG/AGGTTTGACTTGTCTGAGGTTCCT), and found that the difference in estimated copy number was reduced to less than 20% (eNOS mRNA copies per 10^6 cyclophilin copies for the VEGF-High, VEGF-Low, and control Matrigels were 28,978 ± 1442, 7392 ± 901, and 4802 ± 261, respectively).

Multi-gene transcriptional profiling using a master template

There are three different types of NOS: eNOS, iNOS (inducible NOS), and nNOS (neuronal NOS). We generated a NOS gene expression profile by measuring all three NOS genes and the normalizer cyclophilin-A using the standard method in Matrigel samples (Fig. 2a). The three NOS genes were expressed at similar levels in the control Matrigel samples (4.6×10^3 copies of eNOS, 1.7×10^3 copies of iNOS, and 3.5×10^3 copies of nNOS/10^6 copies of cyclophilin) (Fig. 2b). In VEGF-Low Matrigel samples relative to the control, the eNOS expression level increased by 1.54-fold, the iNOS expression level by 1.70-fold, and the nNOS expression level by 1.26-fold. In VEGF-High Matrigel samples relative to the control, a predominant induction of eNOS and iNOS was detected: for every 10^6 copies of cyclophilin mRNA, we obtained approximately 2.8×10^4 copies of eNOS, a 6.2-fold induction; 1.7×10^4 copies of iNOS, a 9.7-fold induction; and 7.3×10^3 copies of nNOS, a 2.1-fold induction (Fig. 2b).

To illustrate the master-template approach, two cDNA templates, *Mm GFAP* and *Mm Flt1*, were arbitrarily selected from the 40 templates in Table 1 that generated less than a 20% difference in copy numbers and were used as master templates to measure the three NOS gene copy numbers. As shown in Fig. 2b, standard curves generated from either *Mm GFAP* or *Mm Flt1* cDNA templates produced less than a 20% difference in estimated copy number for all three genes relative to the standard method.

a

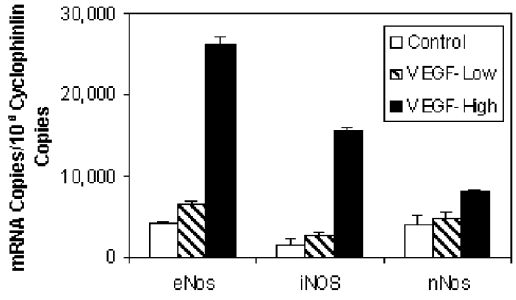

b

	cDNA Templates		
	Standard	*Mm Gfap*	*Mm Flt1*
eNOS			
Control	4545±250	4168±232	4079±228
VEGF-Low	7021±868	6490±812	6363±799
VEGF-High	28230±1424	26378±1348	26004±1334
iNOS			
Control	1736±315	1531±374	1493±366
VEGF-Low	2958±483	2637±439	2577±431
VEGF-High	16847±767	15540±722	15288±713
nNOS			
Control	3474±573	3862±625	3778±614
VEGF-Low	4367±372	4834±404	4734±397
VEGF-High	7306±346	7306±346	7852±366

Fig. 2. Multi-gene transcriptional profiles obtained through precision and master-template approaches. (a) Results using the high-precision approach, in which eNOS, iNOS, and nNOS cDNA templates and their respective primer sets were used to produce standard curve and measure expression of the respective gene. Cyclophilin-A cDNA templates were used to measure copy numbers of the cyclophilin-A normalizer and data is presented as target gene copy number per 10^6 cyclophilin mRNA copies. All three genes increased their expression level significantly in the VEGF-High Matrigel samples whereas the level was only slightly increased in the VEGF-Low Matrigel sample compared to the control. (b) Master-template approach: *Mm GFAP* and *Mm Flt1* cDNA templates and their respective primer sets were used to produce standard curves, which were then used to measured copy numbers of the three NOS genes and the cyclophilin normalizer. Both *Mm GFAP* and *Mm Flt1* templates produced copy numbers that differed less than 20% from the precision results.

Discussion

With high sensitivity (<5 copies), wide dynamic range of quantification (7–8 logarithmic decades), and high precision (<2% standard deviation) (Heid et al., 1996; Jung et al., 2000; Klein, 2002), real-time PCR has come into wide use as a bio-instrument for gene expression measurement in pathology (Alizadeh et al., 2000; Rickman et al., 2001; Simkhovich et al., 2003). The unique advantages of real-time PCR enabled us to pioneer a method for quantitative transcriptional profiling of multi-gene panels to fingerprint biological tissues by measuring mRNA copy numbers through gene-specific cDNA templates (Shih et al., 2002). To improve the technique's experimental throughput, we have now developed an approach that uses a single master template for measuring all genes of interest, thereby significantly increasing experimental throughput when studying panels with large numbers of genes.

Real-time PCR quantification is based on the concepts of the cycle threshold (Ct), defined as the cycle number at which fluorescence reaches a certain threshold value, and the standard curve, which plots threshold cycle as a function of initial abundance (Jung et al., 2000; Liu and Saint, 2002; Wilhelm and Pingoud, 2003). The fluorescence signal is proportional to the quantity of product, which in the absence of saturation rises exponentially and is related to the initial quantity after n cycles according to the formula $Nn = N_0 \times (1 + E)^n$, where E is the efficiency of amplification. In the absence of saturation, therefore, Ct values would increase by 1.0 with each $(1 + E)$-fold dilution of the initial abundance(Pfaffl et al., 2002). Equivalently, between ten-fold serial dilutions, the efficiency is related to the change in Ct by the formula $E = 10^{\frac{-1}{\Delta Ct}} - 1$ (Liu and Saint, 2002; Wilhelm and Pingoud, 2003).

The fluorescence signal does saturate, however, due in part to consumption of reagents and accumulation of pyrophosphate molecules to block enzyme activity (Liu and Saint, 2002; Wilhelm and Pingoud, 2003). Saturation causes the rate of increase in the fluorescence signal to decline over the course of amplification and approach zero as the fluorescence signal plateaus. Mild saturation effects are typically apparent even as the fluorescence signal appears above the background (in the form of a reduced slope to the fluorescence curve). The magnitude of apparent saturation effects can also be affected by such experimental variables as the choice of vendor for reagents (data not shown).

With no saturation and 100% PCR efficiency, the standard curve would be linear with a slope of 3.32 (i.e., Ct would increase by 3.32 with each 10-fold dilution). In our hands, the measured PCR efficiency of fifty-nine different cDNA templates ranged from 90% to 103%, with measured efficiencies over 100% a sign of significant saturation effects. A naïve calculation might predict that abundance increases as $(1 + E)^n$, so that an efficiency range of 90% to 103% would, over 30 PCR cycles, yield a difference in estimated copy numbers of a factor of $(2.03/1.9)^{30}$, or 630%. However, in practice, the maximum percentage difference in measured copy number, even using templates whose efficiency varies significantly, is less than 50%. This result is primarily due to the inverse correlation of the slope of a standard curve with its intercept; the increase in estimated copy number due to a higher intercept partially balances the decrease in estimated copy number due to a decreased efficiency as indicated by the standard curve slope. It is little appreciated by most practitioners that standard curve intercepts are inversely correlated with slopes, so that naïve calculations like the one above greatly overestimate the dependence of estimated initial abundance on efficiency.

Although our study only has 59 cDNA templates and the number of primer sets with complementary 5′-end bases may be too low for a definitive conclusion, quantification errors seem to be significantly increased by complementary at the 5′-ends of primers (e.g., C/G or A/T combinations). A possible mechanism for such errors may be non-specific extension by the Taq polymerase of primers joined initially and transiently at the 5′-ends. The resulting extended primers can be amplified in the PCR process and can form long double-stranded sections that contribute a 'false-positive' fluorescence signal. The extended primers may also be less likely to anneal to amplicons, reducing the availability of primers. When 5′-end primer nucleotides are complementary, the measured PCR amplification efficiencies often exceed 100% (Table 1); this supports the idea that the dominant mechanism for quantification errors is a false-positive fluorescence signal that grows with cycle number and is independent of the starting quantity of the amplicons. Such a cycle-number-dependent, amplicon-quantity-independent signal can lead to measured efficiencies of more than 100%. We conclude that, if a master template is to be used, it is desirable for its primers to be designed to minimize the likelihood of primer linkage at the 5′-end by eliminating complementarity between the 5′-ends of the forward and reverse primers. This principle for 5′-end primer design has not previously been reported in the literature.

If designing primers without 5′-end complementarities can reduce the difference in estimated copy number from using the master-template method to less than 20%, then quantification errors due to use of the master-template approach may be acceptable for most laboratory purposes, especially since every PCR run typically yields 10–20% discrepancies due to various sources of experimental error including instrument and pipetting errors (Ginzinger, 2002).

Other issues affecting the reliability of the obtained data are the choice of the housekeeping gene and sample quality (Thellin et al., 1999). Since not all starting materials for cDNA preparation are free of RNA degradation, and not all proposed housekeeping genes, such as GAPDH and actin (Goidin et al., 2001; Zhu et al., 2001), are constant across samples, it is important to monitor both cDNA quality and the expression of the chosen housekeeping gene by calibrating with 18S RNA.

Nitric oxide (NO) is responsible for vasodilation and mediates a multiplicity of processes involved in angiogenesis including endothelial cell survival, proliferation, migration, and interaction with the extracellular matrix (Murohara et al., 1999; Noiri et al., 1998). VEGF up-regulates the endothelial expression of NO synthase (NOS) (Hood et al., 1998; van der Zee et al., 1997). As we also observed in this study, the greater degree of mouse skin neovascularization induced by VEGF-High transfectants was accompanied by higher levels of eNOS expression. By generating an expression profile of the three NOS genes, eNOS, iNOS, and nNOS, we were able to examine the relationship between the three NOS genes in Matrigel samples. We found that in the VEGF-High transfectant, eNOS was the most abundant NOS while iNOS was the most strongly induced. The information of three NOS gene relationship obtained through this multi-gene profile provides insights as to which NOS gene will play a more predominant role when all three genes are expressed.

In summary, our study indicates that with properly designed primers, fresh reagents, good selection of a master-template standard, reliable instrumentation, and consistent data analysis, the master-template method for real-time PCR gene quantification will yield reliable mRNA copy numbers. By avoiding cloning of specific templates for every target gene, the master-template method increases experimental throughput, reduces errors introduced through template variations, and makes it easier to compare data from different assays. By enabling reliable inter-gene abundance comparisons in multi-gene panels, the technique provides a measure of the overall state of gene expression that will help to identify genes of biological importance. As a high-throughput technique capable of measuring the

expression of large panels of genes, it will be valuable not only for fingerprinting biological states, but also for observing the dynamics of the gene–protein network during disease processes and for validating DNA-microarray data. Concerns over accuracy may be addressed by turning to the standard approach of gene-specific templates after the master-template approach has first identified a smaller set of genes of interest.

Acknowledgments

We thank Sam Bride, Erin Crete, and Luhua Shen for technical contributions, Dr. Donald Senger for help with Matrigel tumor studies, and Dr. Paul Jaminet for helpful discussions regarding the mathematics of real-time PCR quantification and the influence of saturation effects.

References

Alizadeh, A.A., Eisen, M.B., Davis, R.E., Ma, C., Lossos, I.S., Rosenwald, A., Boldrick, J.C., Sabet, H., Tran, T., Yu, X., Powell, J.I., Yang, L., Marti, G.E., Moore, T., Hudson Jr., J., Lu, L., Lewis, D.B., Tibshirani, R., Sherlock, G., Chan, W.C., Greiner, T.C., Weisenburger, D.D., Armitage, J.O., Warnke, R., Levy, R., Wilson, W., Grever, M.R., Byrd, J.C., Botstein, D., Brown, P.O., Staudt, L.M., 2000. Distinct types of diffuse large B-cell lymphoma identified by gene expression profiling. Nature 403, 503–511.

Bassett Jr., D.E., Eisen, M.B., Boguski, M.S., 1999. Gene expression informatics—It's all in your mine. Nat. Genet. 21, 51–55.

Brown, P.O., Botstein, D., 1999. Exploring the new world of the genome with DNA microarrays. Nat. Genet. 21, 33–37.

Clarke, P.A., te Poele, R., Wooster, R., Workman, P., 2001. Gene expression microarray analysis in cancer biology, pharmacology, and drug development: progress and potential. Biochem. Pharmacol. 62, 1311–1336.

Crnogorac-Jurcevic, T., Efthimiou, E., Nielsen, T., Loader, J., Terris, B., Stamp, G., Baron, A., Scarpa, A., Lemoine, N.R., 2002. Expression profiling of microdissected pancreatic adenocarcinomas. Oncogene 21, 4587–4594.

Ding, C., Cantor, C.R., 2004. Quantitative analysis of nucleic acids—The last few years of progress. J. Biochem. Mol. Biol. 37, 1–10.

Ginzinger, D.G., 2002. Gene quantification using real-time quantitative PCR: an emerging technology hits the mainstream. Exp. Hematol. 30, 503–512.

Goidin, D., Mamessier, A., Staquet, M.J., Schmitt, D., Berthier-Vergnes, O., 2001. Ribosomal 18S RNA prevails over glyceraldehyde-3-phosphate dehydrogenase and beta-actin genes as internal standard for quantitative comparison of mRNA levels in invasive and noninvasive human melanoma cell subpopulations. Anal. Biochem. 295, 17–21.

Heid, C.A., Stevens, J., Livak, K.J., Williams, P.M., 1996. Real time quantitative PCR. Genome Res. 6, 986–994.

Hood, J.D., Meininger, C.J., Ziche, M., Granger, H.J., 1998. VEGF upregulates ecNOS message, protein, and NO production in human endothelial cells. Am. J. Physiol. 274, H1054–H1058.

Jung, R., Soondrum, K., Neumaier, M., 2000. Quantitative PCR. Clin. Chem. Lab. Med. 38, 833–836.

Klein, D., 2002. Quantification using real-time PCR technology: applications and limitations. Trends Mol. Med. 8, 257–260.

Liu, W., Saint, D.A., 2002. A new quantitative method of real time reverse transcription polymerase chain reaction assay based on simulation of polymerase chain reaction kinetics. Anal. Biochem. 302, 52–59.

Mah, N., Thelin, A., Lu, T., Nikolaus, S., Kuhbacher, T., Gurbuz, Y., Eickhoff, H., Kloppel, G., Lehrach, H., Mellgard, B., Costello, C.M., Schreiber, S., 2004. A comparison of oligonucleotide and cDNA-based microarray systems. Physiol. Genomics 16, 361–370.

Miyazato, A., Ueno, S., Ohmine, K., Ueda, M., Yoshida, K., Yamashita, Y., Kaneko, T., Mori, M., Kirito, K., Toshima, M., Nakamura, Y., Saito, K., Kano, Y., Furusawa, S., Ozawa, K., Mano, H., 2001. Identification of myelodysplastic syndrome-specific genes by DNA microarray analysis with purified hematopoietic stem cell fraction. Blood 98, 422–427.

Morrison, T.B., Weis, J.J., Wittwer, C.T., 1998. Quantification of low-copy transcripts by continuous SYBR Green I monitoring during amplification. BioTechniques 24, 954–958, 960, 962.

Murohara, T., Witzenbichler, B., Spyridopoulos, I., Asahara, T., Ding, B., Sullivan, A., Losordo, D.W., Isner, J.M., 1999. Role of endothelial nitric oxide synthase in endothelial cell migration. Arterioscler., Thromb., Vasc. Biol. 19, 1156–1161.

Noiri, E., Lee, E., Testa, J., Quigley, J., Colflesh, D., Keese, C.R., Giaever, I., Goligorsky, M.S., 1998. Podokinesis in endothelial cell migration: role of nitric oxide. Am. J. Physiol. 274, C236–C244.

Pfaffl, M.W., Horgan, G.W., Dempfle, L., 2002. Relative expression software tool (REST) for group-wise comparison and statistical analysis of relative expression results in real-time PCR. Nucleic Acids Res. 30, e36.

Rickman, D.S., Bobek, M.P., Misek, D.E., Kuick, R., Blaivas, M., Kurnit, D.M., Taylor, J., Hanash, S.M., 2001. Distinctive molecular profiles of high-grade and low-grade gliomas based on oligonucleotide microarray analysis. Cancer Res. 61, 6885–6891.

Shih, S.C., Robinson, G.S., Perruzzi, P., Calvo, A., Desai, K., Green, J., Ali, I., Smith, L.E., Senger, D., 2002. Molecular profiling of angiogenesis markers. Am. J. Pathol. 161, 35–41.

Shih, S.C., Ju, M., Liu, N., Smith, L.E., 2003a. Selective stimulation of VEGFR-1 prevents oxygen-induced retinal vascular degeneration in retinopathy of prematurity. J. Clin. Invest. 112, 50–57.

Shih, S.C., Ju, M., Liu, N., Mo, J.R., Ney, J.J., Smith, L.E., 2003b. Transforming growth factor {beta}1 induction of vascular endothelial growth factor receptor 1: mechanism of pericyte-induced vascular survival in vivo. Proc. Natl. Acad. Sci. U. S. A. 100, 15859–15864.

Simkhovich, B.Z., Kloner, R.A., Poizat, C., Marjoram, P., Kedes, L.H., 2003. Gene expression profiling—A new approach in the study of myocardial ischemia. Cardiovasc. Pathol. 12, 180–185.

Thellin, O., Zorzi, W., Lakaye, B., De Borman, B., Coumans, B., Hennen, G., Grisar, T., Igout, A., Heinen, E., 1999. Housekeeping genes as internal standards: use and limits. J. Biotechnol. 75, 291–295.

Trandinh, C.C., Pao, G.M., Saier Jr., M.H., 1992. Structural and evolutionary relationships among the immunophilins: two ubiquitous families of peptidyl–prolyl *cis–trans* isomerases. FASEB J. 6, 3410–3420.

van der Zee, R., Murohara, T., Luo, Z., Zollmann, F., Passeri, J., Lekutat, C., Isner, J.M., 1997. Vascular endothelial growth factor/vascular permeability factor augments nitric oxide release from quiescent rabbit and human vascular endothelium. Circulation 95, 1030–1037.

Wilhelm, J., Pingoud, A., 2003. Real-time polymerase chain reaction. ChemBioChem 4, 1120–1128.

Wittwer, C.T., Herrmann, M.G., Moss, A.A., Rasmussen, R.P., 1997. Continuous fluorescence monitoring of rapid cycle DNA amplification. BioTechniques, 22, 130–131, 134–138.

Yauk, C.L., Berndt, M.L., Williams, A., Douglas, G.R., 2004. Comprehensive comparison of six microarray technologies. Nucleic Acids Res. 32, e124.

Zhu, G., Chang, Y., Zuo, J., Dong, X., Zhang, M., Hu, G., Fang, F., 2001. Fudenine, a C-terminal truncated rat homologue of mouse prominin, is blood glucose-regulated and can up-regulate the expression of GAPDH. Biochem. Biophys. Res. Commun. 281, 951–956.